EXPERIMENTAL STUDY ON THE EFFECT OF THE IGNITION LOCATION ON VENTED DEFLAGRATION OF HYDROGEN-AIR MIXTURES IN ENXLOSURE

Yoon, U.G.[1], Kim, Y.K.[1], Park, B.J.[1], Kim, J.S.[1] and Kim, W.K.[2]
[1] Department of Fire Safety Research/Hydrogen-infra. Research Cluster,
Korea Institute of Civil Engineering and Building Technology (KICT),
64, 182Beon-Gil, Mado-Ro, Mado-Myeon, Hwaeong-Si, Gyeonggi-Do, 18544, South Korea,
yoonunggi@kict.re.kr, yangkyunkim@kict.re.kr, templer83@kict.re.kr, kkpp9810@kict.re.kr
[2] Reactive Gas Dynamics Laboratory, Hiroshima University,
4-1, Kagamiyama 1chome, Higashi-Hiroshima, 739-8527, Japan,
kimwk@hiroshima-u.ac.jp

ABSTRACT

No countermeasures exist for accidents that might occur in hydrogen-based facilities (leaks, fires, explosions, etc.). In South Korea, discussions are underway regarding measures to ensure safety from such accidents, such as the construction of underground hydrogen storage tank facilities. However, explosion vents with a minimum ventilation area are required in such facilities to minimize damage to buildings and other structures due to accidental explosions. These explosion vents allow the generated overpressure and flames to be safely dispersed outside; however, a safe separation distance must be secured to minimize damage to humans. This study aimed to determine the safe separation distance to minimize human damage after analyzing the dispersed overpressure and flame behavior following a vent explosion. Explosion experiments were conducted to investigate the influence of the ignition source location on internal and external overpressure and external flame behavior using a cuboid concrete structure with a volume of 20.33 m^3 filled with a hydrogen-air mixture (29.0 vol.%). The impact on overpressure and flame was increased with the increasing distance of the ignition source from the vent. Importantly, depending on the ignition location the incident pressure was up to 24.4 times higher, while the reflected pressure was 8.7 times higher. Additionally, a maximum external overpressure of 30.01 kPa was measured at a distance of 2.4 m from the vent, predicting damage to humans at the “Injury” level (1 % fatality probability). Whereas, no significant damage would occur at a distance of 7.4 m or more from the vent.

1.0 INTRODUCTION

Governments worldwide are declaring to pursue carbon neutrality in response to the climate change crisis and global warming. In line with this trend, the Korean government announced its "declaration of commitment to carbon neutrality" and the "2050 Carbon Neutrality Implementation Strategy" covering all energy-related sectors (energy supply, industry, transportation, buildings, etc.) to achieve carbon neutrality by 2050 [1]. This strategy promotes energy system innovation centered on clean energy, with hydrogen receiving worldwide attention as a form of indispensable clean energy. Consequently, the trend is shifting to a "hydrogen economy" using hydrogen as the main energy source, which is expected to be led by hydrogen production, transportation, storage, and mobility (hydrogen vehicles and charging stations) through hydrogen fuel cell power generation industries [2,3]. However, countermeasures for avoiding accidents that can occur in hydrogen energy infrastructure and related facilities (leaks, fires, explosions, etc.) are lacking. Therefore, the establishment of countermeasures to minimize such accidents and potential human damage is urgently needed. In this regard, the Korean government is discussing the construction of underground hydrogen storage tank facilities to ensure the safety of the population from accidents due to hydrogen leaks, fires, and explosions. For the construction of underground hydrogen storage tank facilities, measures must be taken to minimize the damage to buildings and other structures due to accidental explosions within the facility. Explosion vents are widely used as such countermeasures; for confined spaces in particular, it is necessary to design explosion vents with at least a minimum ventilation area. Such explosion vents allow the outside dispersion of the overpressure and flames generated by accidental

explosions. However, even in this scenario, a safe separation distance must be secured to minimize human damage caused by the dispersed overpressure and flames.

Various experimental studies have been conducted on the structure and function of explosion vents [4-10]. Bauwens et al. [4,5] carried out vent explosion experiments in chambers filled with various gas-air mixtures. They set the parameters of vent size, gas concentration, gas type, and ignition location, and investigated the influence of these parameters on the pressure development of diffusion flames in the vent. Wang et al. [6] used a rectangular container with a vent at the top to experimentally investigate the pressure rise and flame behavior during vent explosions of hydrogen-air mixtures. They reported that the maximum length and duration of the external flame increased and decreased, respectively, with the increasing hydrogen concentration. Skjold et al. [7] performed vent explosion experiments using hydrogen-air mixtures in a 20-ft container to investigate the effects of congestion on homogeneous and heterogeneous mixtures. They found that internal congestion greatly increased the maximum reduced explosion pressure of vented deflagrations compared with that in empty enclosures. Using a manhole model, Li et al. [8] conducted manhole explosion experiments and investigated the influence of methane concentration, ignition location, and manhole cover weight on the peak pressure caused by the manhole explosion. Tang et al. [9] investigated pressure-time history and flame behavior using 7 different vent sizes with vent coefficients (K_V) ranging from 3.57 to 25.00 during vent explosions in a cuboid chamber filled with a hydrogen-air mixture. Liu et al. [10] performed explosion experiments in a vertical rectangular duct with a vent at the top, examining the effect of the vent coefficient (K_V) on flame propagation and pressure rise during vent explosions of hydrogen-methane-air mixtures. Most of these studies focused on the influence of the vent coefficient on flame propagation and pressure rise during vent explosions. However, the impact of roof vent explosions at adjacent distances has not been investigated. Additionally, as most studies focused on predicting explosion pressure and flame behavior caused by vent explosions in chambers with side vents, they are limited in identifying the level of human damage at adjacent distances caused by roof vent explosions and predicting the safe separation distance from the explosion vent [11-16].

Therefore, this study aimed to determine the safe separation distance for minimizing human damage after analyzing the overpressure and flame behavior dispersed outside due to vent explosion. We carried out an explosion experiment in a full-scale cuboid concrete structure (20.33 m^3) with a vent (1.13 m^2) at the top, filled with a hydrogen-air mixture (29.0 vol.%). The overpressure inside and outside the structure and flame behavior were analyzed according to the ignition source location, and the safe separation distance was predicted based on the level of human damage.

2. METHODS AND MATERIALS

2.1 Experimental Structures and Measuring Instruments

As shown in Fig. 1, we conducted the vent explosion experiments using a full-scale (20.33 m^3) concrete structure with the following dimensions: L: 4800 mm, W: 2800 mm, H: 2800 mm. An outline of the concrete structure is provided in Fig. 2 and Table 1. The explosion vent had a rectangular shape (L: 750 mm, and H: 1500 mm) and was placed symmetrically in the center of the roof of the concrete structure. To prevent hydrogen gas injected into the experimental structure from leaking through the vent, a thin vinyl sheet (thickness of 0.2 mm) as used to completely seal the vent. The vent coefficient, which is given by the following equation: $V^{2/3}/A_V$ (V: volume of enclosed space, A_V: area of the vent), was 6.62.

Table 1. Overview of experimental structure.

Type	Structures					Roof vent			
Concrete structures	Dimensions (m)			Thickness (m)	Volume (m^3)	Dimensions (m)		Area A_V (m^2)	Coefficient K_V ($V^{2/3}/A_V$)
	L	W	H	W	V	L	H		
	4.8	2.8	2.8	0.3	20.33	0.75	1.5	1.13	6.62

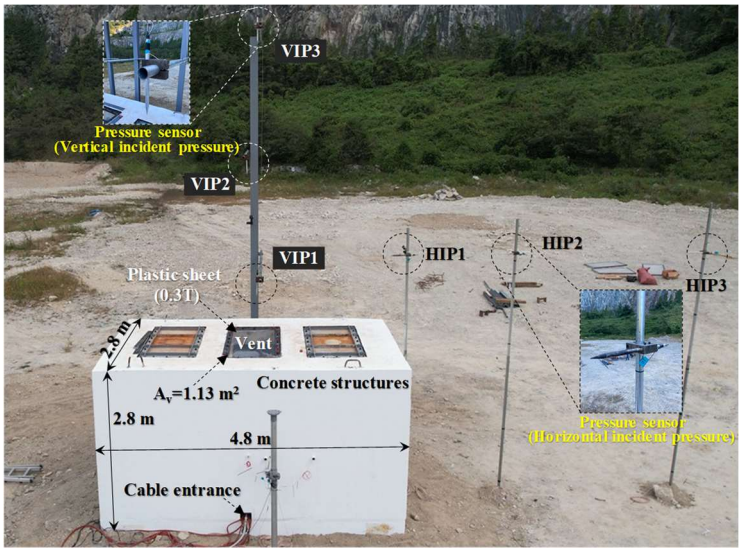

Figure 1. Experimental structure used for hydrogen-air mixture vented deflagration tests

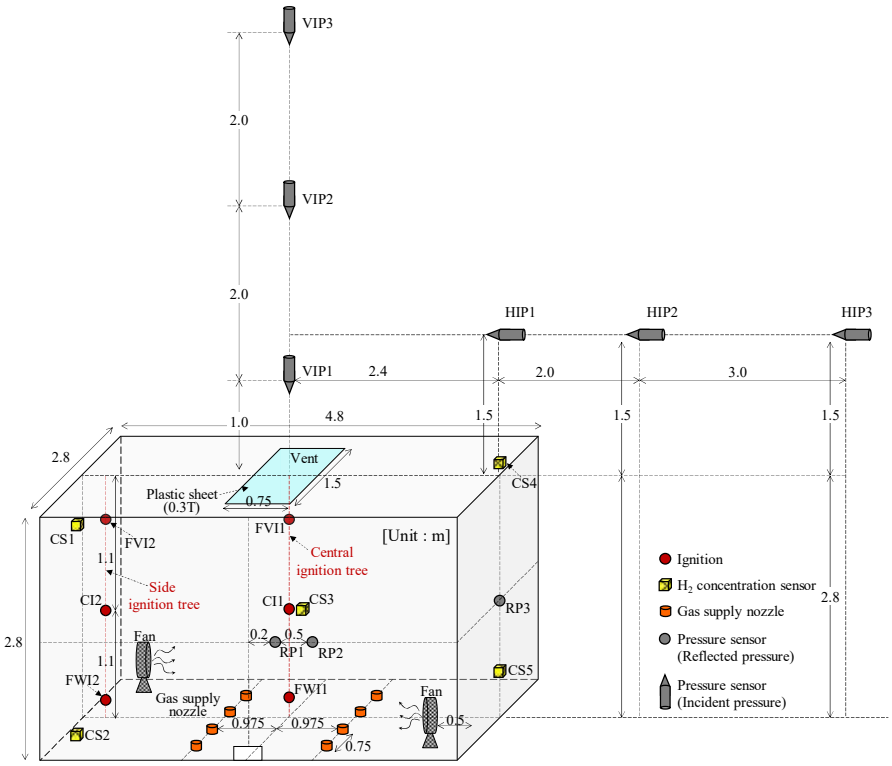

Figure 2. Experimental structure used for hydrogen-air mixture vented deflagration tests

Fig. 2 shows the status of the measuring devices used for the vent explosion experiments. Three vertical incident pressure gauges (VIP1–3) were installed at 1.0 m (VIP1), 3.0 m (VIP2), and 5.0 m (VIP3) above the center of the vent plane to measure the explosion pressure radiating from the vent. Likewise, 3 horizontal incident pressure gauges (HIP1–3) were installed at 2.4 m (HIP1), 4.4 m (HIP2), and 7.4 m (HIP3) to the right at a height of 1.5 m from the center of the vent plane to measure the effects of a vent explosion on people at adjacent distances. Of note, 3 reflective pressure gauges (RP1–3) were installed in the central part of the inner wall (RP1), the central 1/4 point (RP2), and the central part of the right wall (RP3) to measure the internal explosion pressure. Importantly, 6 ignition devices were installed inside the structure to investigate the influence of the ignition location on vent explosions. Among them, 3 ignition devices (central ignition tree) were installed at 200 mm (front-

vent ignition, FVI1), 1100 mm (central ignition, CI1), and 2000 mm (floor-wall ignition, FWI1) below the center of the vent plane. At the same heights as the central ignition tree (FVI1, CI1, and FWI1), another 3 ignition devices (FVI2, CI2, and FWI2) were installed 1900 mm to the left (side ignition tree). Five hydrogen concentration sensors (CS1–5) were installed at the upper (CS1, 4) and lower (CS2, 5) ends of the diagonal in the X direction and at the center (CS3) to monitor the hydrogen concentration in the entire internal space. Hydrogen gas was supplied through 8 nozzles installed at the bottom of the structure using a mass flow controller (MKP, TSM-D260). Explosion-proof fans were placed at both ends of the diagonal to ensure the homogeneous concentration of the hydrogen-air mixture inside. Finally, a thermal imaging camera was placed in front of the experimental structure to record the external flame behavior according to the ignition location.

2.2 Experimental Conditions and Method

Table 2 shows the conditions of the ventilation explosion experiments using a hydrogen-air mixture according to the ignition location. To examine the influence of the ignition location on explosion behavior, we tested a total of 6 ignition locations in our ventilation explosion experiments, including a central ignition tree (front-vent ignition1, central ignition1, and floor-wall ignition1) and a side ignition tree (front-vent ignition2, central ignition2, and floor-wall ignition2). In addition, we set the hydrogen concentration at 29.0 %, corresponding to an equivalence ratio (Ø) of 1.0, in which the hydrogen-air combustion reaction proceeds efficiently. We uniformly applied these vent conditions with an area of 1.13 m^2 (L 0.75 x H 1.5 m), corresponding to the required minimum vent area (A_{v0} = 1.09 m^2) as presented in Eq. (1) of NFPA 68 (2013) [17] and KFS 750 (1998) [18] in all performed experiments. We tested the effect of each ignition location once.

$$A_{v0} = A_s \frac{\left[1-\left(\frac{P_{red}+1}{P_{max}+1}\right)^{1/\gamma b}\right]}{\left[\left(\frac{P_{red}+1}{P_{max}+1}\right)^{1/\gamma b}-\delta\right]} \frac{S_u \rho_u}{G_u} \frac{\lambda}{C_d}, \quad (1)$$

where A_{v0} – the vent area calculated, m^2; A_s – enclosure internal surface area, m^2; P_{red} – maximum pressure developed in a vented enclosure during a vented deflagration, bar-g; S_u – fundamental burning velocity of gas-air mixture, m/s; ρ_u – mass density of unburned gas-air mixture, kg/m^3; λ – ratio of gas-air mixture burning velocity; G_u – unburned gas-air mixture sonic flow mass flux, kg/m^2-s; C_d – vent flow discharge coefficient; P_{max} – maximum pressure, bar-g; and γb – ratio of enclosure pressure prior to ignition, bar-g.

Table 2. Summary of experimental conditions.

Test no.	Vent condition	Vent coefficient	Ignition location		Concentration of hydrogen
1	A_V= 1.13m^2	K_V= 6.62	Central ignition tree	Front-vent ignition 1	29.0 %
2				Central ignition 1	
3				Floor-wall ignition 1	
4			Side ignition tree	Front-vent ignition 2	
5				Central ignition 2	
6				Floor-wall ignition 2	

The experimental process involved sealing the explosion vent with a 0.2-mm-thick vinyl sheet to create a sealed space, allowing the supply of the hydrogen gas. The hydrogen gas was supplied through 8 gas supply nozzles (Ø = 2.8 mm) installed on the floor, and its supply in the sealed structure at a constant flow rate was controlled using a mass flow controller (MKP, TSM-D260). The supplied hydrogen gas was monitored in real-time using hydrogen concentration sensors, and was stopped when the desired range was reached within ±3.0 %. Subsequently, 2 explosion-proof fans installed in the structure thoroughly mixed the hydrogen and air in the compartment. After stopping the explosion-proof fans and stabilizing the hydrogen concentration within the compartment, various measurement

data loggers were activated, and the mixed gas was ignited using an electric spark ignition system installed in the structure. Following the explosion that occurred immediately after ignition, both the incident and reflected pressure values were measured in units of time (microsecond, μs: millionths of a second) using pressure sensors connected to the data loggers. The external flame behavior was also recorded using a thermal imaging camera placed in front of the experimental structure.

3. RESULTS AND DISCUSSION

3.1 Timing of Hydrogen Concentration of Roof Vented Deflagrations

The plots of hydrogen concentration at different ignition locations within the experimental structure are shown in Fig. 3(A) and (B). We determined the hydrogen concentration by calculating the average value of measurements from the 5 hydrogen concentration sensors (CS1–5) installed in the structure. Of note, the hydrogen concentration plots are divided into Steps 1–3. Step 1 is the section where the hydrogen concentration is controlled within ±3.0 % of the target value through the nozzles installed in the structure. Step 2 is the section just before ignition where the supply of hydrogen is stopped, and a homogeneous hydrogen concentration is created through the thorough mixing of hydrogen and air by the installed explosion-proof fans. Step 3 is the section from ignition to when the hydrogen concentration drops to 0.0 vol.%.

First, we properly controlled the supply of hydrogen to reach the target value of hydrogen concentration during Step 1. During Step 2, we maintained a stable state within ±3.0 % of the target value (29.0 vol.%). Whereas, we observed a sharp drop in hydrogen concentration to approximately 0.0 vol.% immediately after ignition in Step 3. These results confirmed that the explosion occurred after the hydrogen concentration was properly controlled.

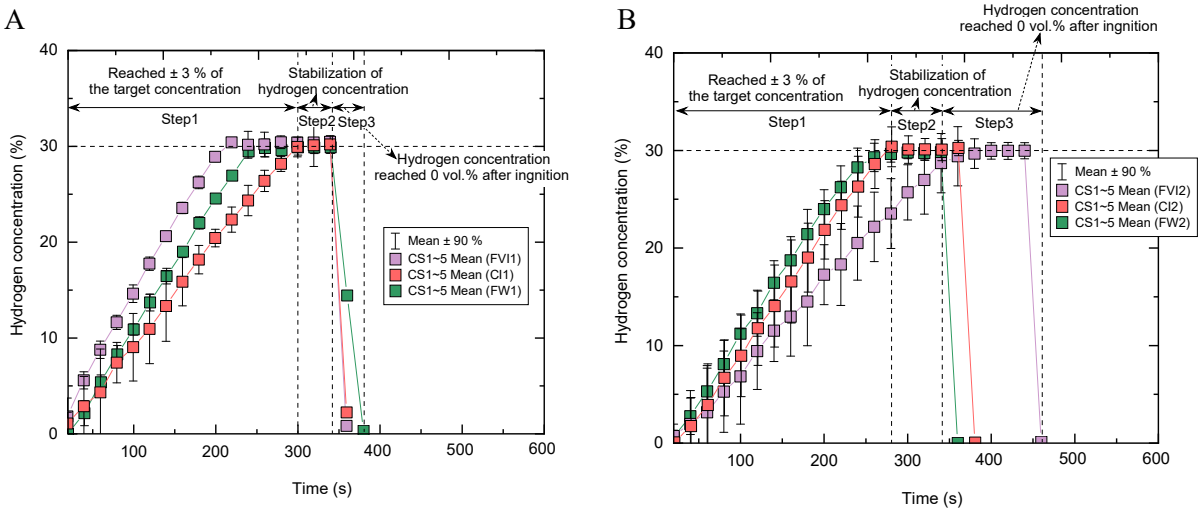

Figure 3. Hydrogen concentration in the structure
A: Central ignition tree (FVI1, CI1 and FWI1); B: Side ignition tree (FVI2, CI2 and FWI2)

3.2 Overpressure Recordings in Roof Vent Deflagration

3.2.1 Vertical incident pressure recordings in vented deflagration

We divided the vertical incident pressure (VIP1–3) recordings according to the ignition location into center (FVI2, CI2, and FWI2) and side (FVI2, CI2, and FWI2) ignition tree data and present them in Fig. 4(A)-(C) and Fig. 5(A)-(C), respectively, along with the recorded overpressure and impulse values. The reflected pressure (RP3) data for each ignition tree are shown in Fig. 4(D) and Fig 5(D), respectively. We observed that in the case of FVI1 ignition of the central ignition tree (FVI1, CI1, and FWI1), a small maximum pressure of 0.96 kPa was measured at VIP1 installed directly above the vent, followed by recordings of sequential maximum pressures of 0.32 kPa and 0.20 kPa at VIP2 and

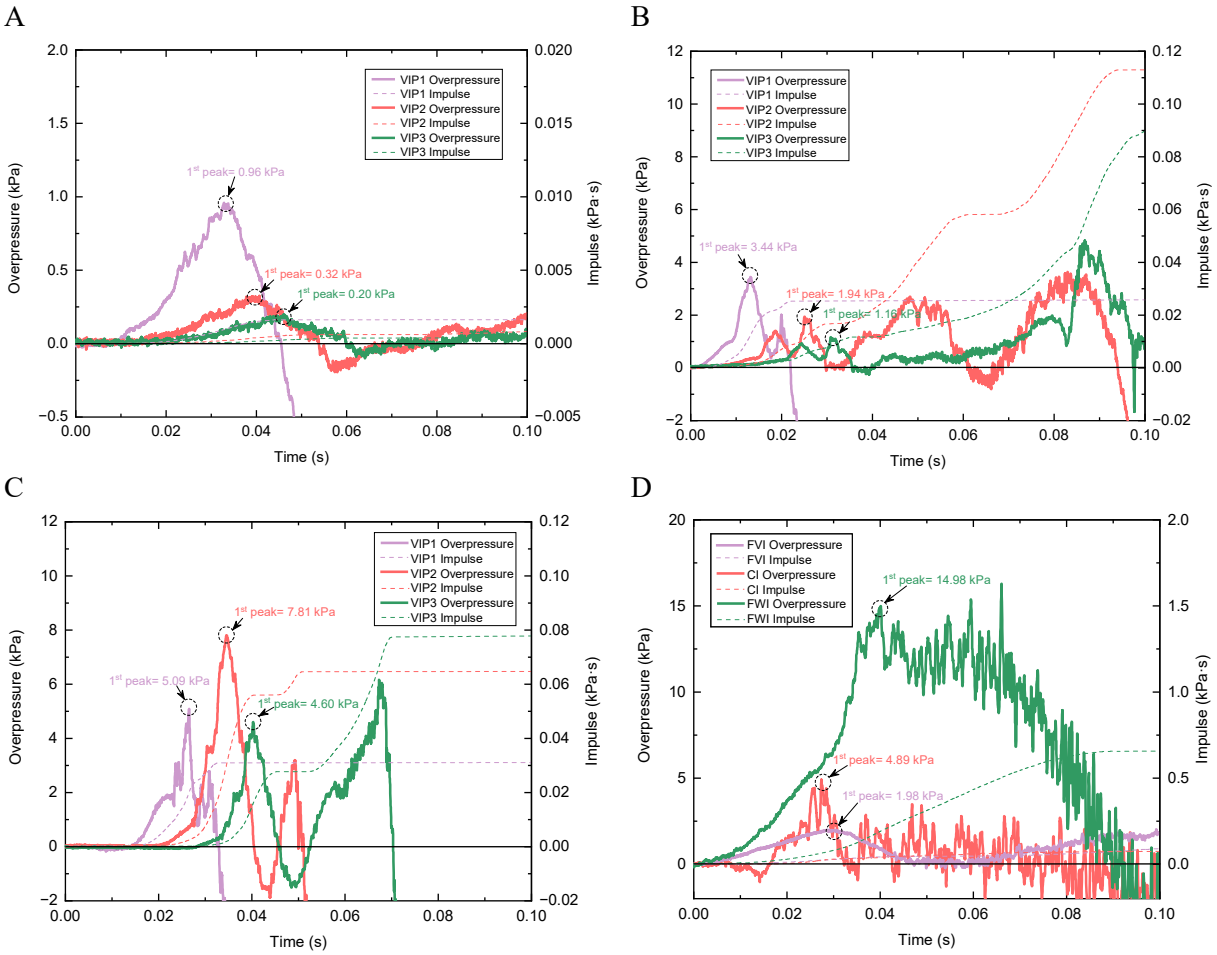

Figure 4. Incident and reflected pressure values according to the ignition location (Central ignition tree) A: VIP1–3 Overpressure and Impulse (FVI1); B: VIP1–3 Overpressure and Impulse (CI1); C: VIP1–3 Overpressure and Impulse (FWI1); D: RP3 Overpressure and Impulse (Central ignition tree)

VIP3, respectively. In addition, we found that a maximum reflected pressure of 1.98 kPa was measured at RP3. Similar to FVI1, we detected that under CI1 ignition, a maximum pressure of 3.44 kPa was measured at VIP1, followed by recordings of maximum pressures of 1.94 kPa and 1.16 kPa at VIP2 and VIP3, respectively, as well as a maximum reflected pressure of 4.89 kPa measured at RP3. In contrast, under FWI1 ignition, unlike the maximum pressure values recorded with FVI1 and CI1, a maximum pressure of 7.81 kPa was measured at VIP2, followed by recordings of maximum pressures of 5.09 kPa and 4.60 kPa at VIP1 and VIP3, respectively, and a maximum reflected pressure of 14.98 kPa measured at RP3. These results confirmed that the explosion pressure increased as the ignition location moved further away from the vent.

Interestingly, we determined that in the case of FVI2 ignition of the side ignition tree (FVI2, CI2, and FWI2), a maximum pressure of 3.39 kPa was measured at VIP1, which was higher than the maximum pressure (VIP1) recorded at the same height in FVI1 ignition. In addition, we found that the internal maximum reflected pressure showed a pressure difference of more than approximately 2.0 times at 5.44 kPa at RP3. We observed that although the pressure values in the cases of ignition of CI2 and FWI2 showed similar trends in behavior as those in the central ignition tree, the difference in the maxi mum pressure value between the 2 conditions (central and side ignition tree) was large. According to these results, we measured a higher maximum explosion pressure value in the side ignition tree when the ignition location was further away from the vent, even when conducting explosion tests at the same height as the ignition conditions of the central ignition tree, showing a clear difference in the explosion pressure value. This finding confirmed that the maximum explosion pressure was increased as the location of the ignition source was further away from the vent.

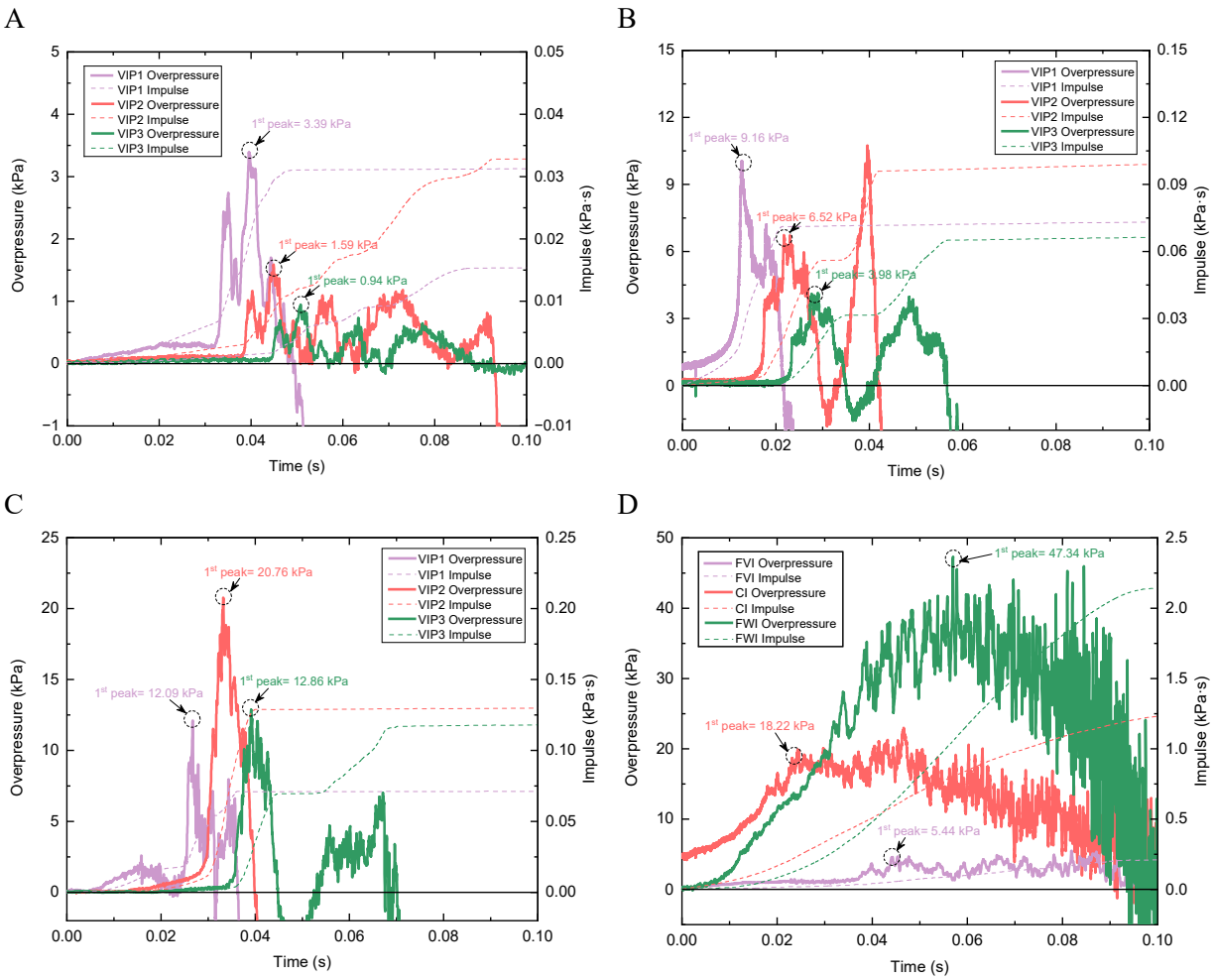

Figure 5. Incident and reflected pressure values according to the ignition location (Side ignition tree) A: VIP1–3 Overpressure and Impulse (FVI2); B: VIP1–3 Overpressure and Impulse (CI2); C: VIP1–3 Overpressure and Impulse (FWI2); D: RP3 Overpressure and Impulse (Central ignition tree)

3.2.2 Horizontal incident pressure recordings in vented deflagration

We also divided the horizontal incident pressure (HIP1–3) recordings according to the ignition location into Central and side ignition tree data, and present them in Fig. 6(A)–(C) and Fig. 7(A-1)–(C-1), respectively, along with the recorded overpressure and impulse values. We found that in the case of FVI1 ignition of the central ignition tree, a small maximum pressure of 0.29 kPa was measured at HIP1, located 2.4 m horizontally away from the vent, whereas no pressure from the vent explosion was measured at HIP2 and HIP3. We also detected that under CI1 ignition, a maximum pressure of 1.59 kPa was measured at HIP1, followed by small maximum pressure recordings of 0.95 kPa and 0.58 kPa at HIP2 and HIP3, respectively. However, in the case of FWI1 ignition, we recorded maximum pressure values of 6.03 kPa, 3.02 kPa, and 1.90 kPa at HIP1, HIP2, and HIP3, respectively. Likewise, we observed that under FVI2 ignition of the side ignition tree, a maximum pressure of 1.49 kPa was measured at HIP1, followed by sequential small maximum pressure recordings of 0.89 kPa and 0.52 kPa at HIP2 and HIP3, respectively. Interestingly, these values corresponded to the maximum pressure values recorded under CI1 ignition of the central ignition tree. Similar to FVI2 ignition, we determined that a maximum pressure of 10.70 kPa was measured at HIP1, whereas maximum pressures of 6.75 kPa and 4.44 kPa were measured at HIP2 and HIP3, respectively under CI2 ignition. Of note, we found that although the pressure values under FWI2 ignition showed a similar trend in behavior to those under CI2 ignition, the difference in maximum pressure was approximately 2.0 times higher. Similar to the vertical incident pressure values, these results confirmed that the horizontal incident pressure values measured in the horizontal direction were increased with the increasing distance of the ignition source from the vent.

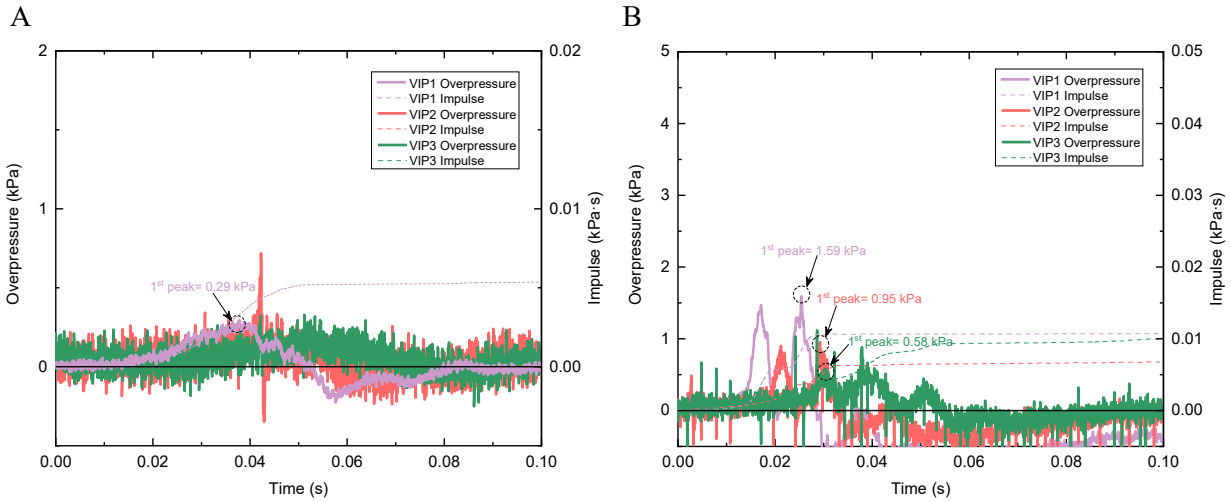

Figure 6. Incident pressure values according to the ignition location (Central ignition tree) A: VIP1–3 Overpressure and Impulse (FVI1); B: VIP1–3 Overpressure and Impulse (CI1)

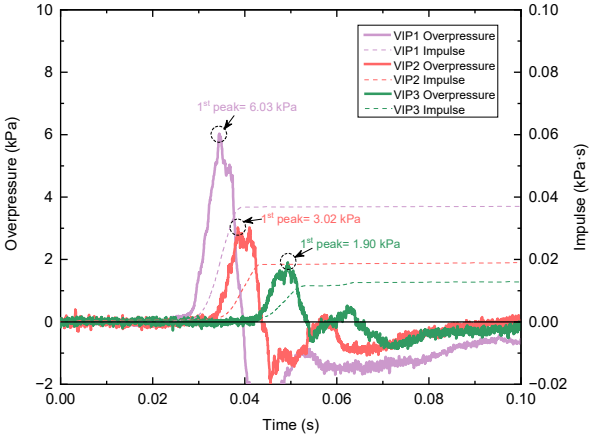

Figure 6. Incident pressure values according to the ignition location (Central ignition tree) C: VIP1–3 Overpressure and Impulse (FWI1)

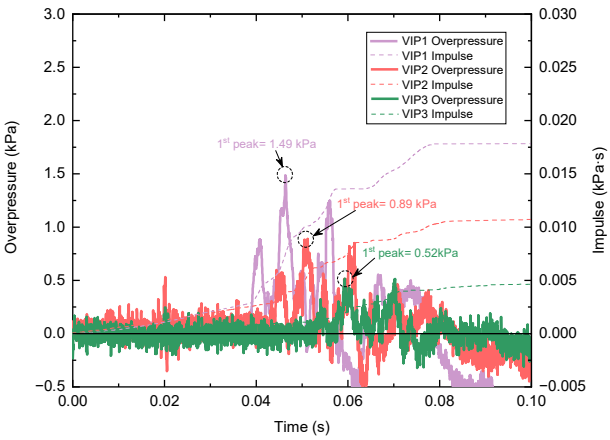

Figure 7. Incident pressure values according to the ignition location (Side ignition tree) A-1: VIP1–3 Overpressure and Impulse (FVI2)

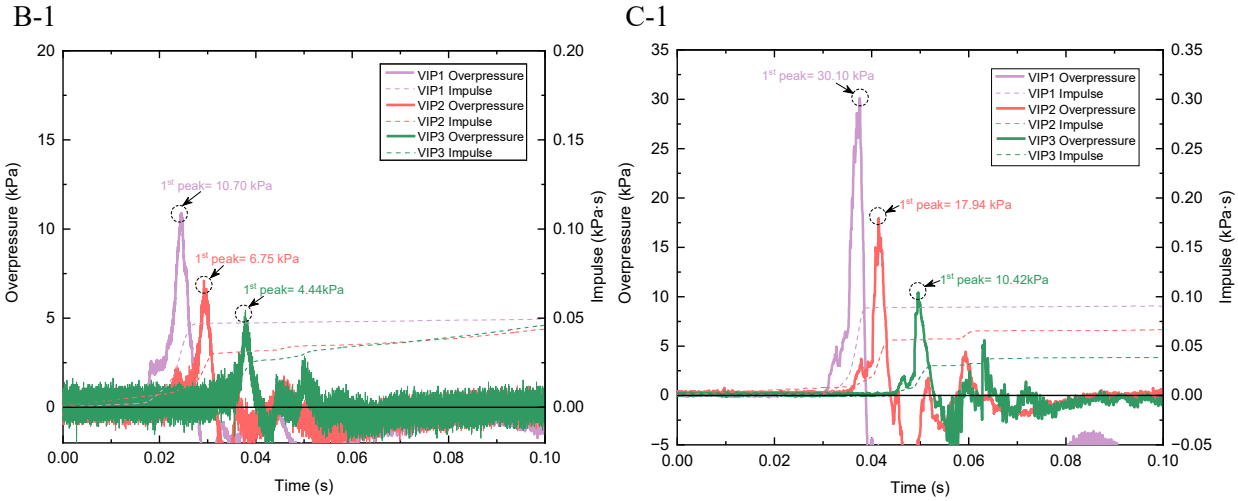

Figure 7. Incident pressure values according to the ignition location (Side ignition tree) B-1: VIP1–3 Overpressure and Impulse (CI2); C-1: VIP1–3 Overpressure and Impulse (FWI2)

3.3 Effect of Ignition Location on Peak Overpressure Value

We divided the peak overpressure values according to ignition location into vertical incident pressure (VIP1–3), horizontal incident pressure (HIP1–3), and reflected pressure (RP3), and present them in Fig. 8(A), (B). Regarding the vertical incident peak overpressure values (VIP1–3), we found that with the increasing distance of the ignition location from the vent, the difference in the maximum explosion pressure value at VIP2 was increased by approximately 24.4 times in the central ignition tree (FVI1 to FWI1) and 13.1 times in the side ignition tree (FVI2 to FWI2). We also confirmed that the maximum explosion pressure value in VIP1–3 was approximately 3.0 times higher in the side ignition tree (FVI2, CI2, and FWI2) compared with that in the central ignition tree (FVI1, CI1, and FWI1). Similar to the above, we observed that among the horizontal incident peak overpressure values (HIP1–3), the difference in the maximum explosion pressure value was increased with the increasing distance of the ignition location, with the maximum explosion pressure of 30.1 kPa being measured at HIP1 under FWI2 ignition (more than 20.0 times higher than that under FVI2 ignition). These results confirmed that the peak overpressure value was increased with the increasing distance of the ignition location from the vent.

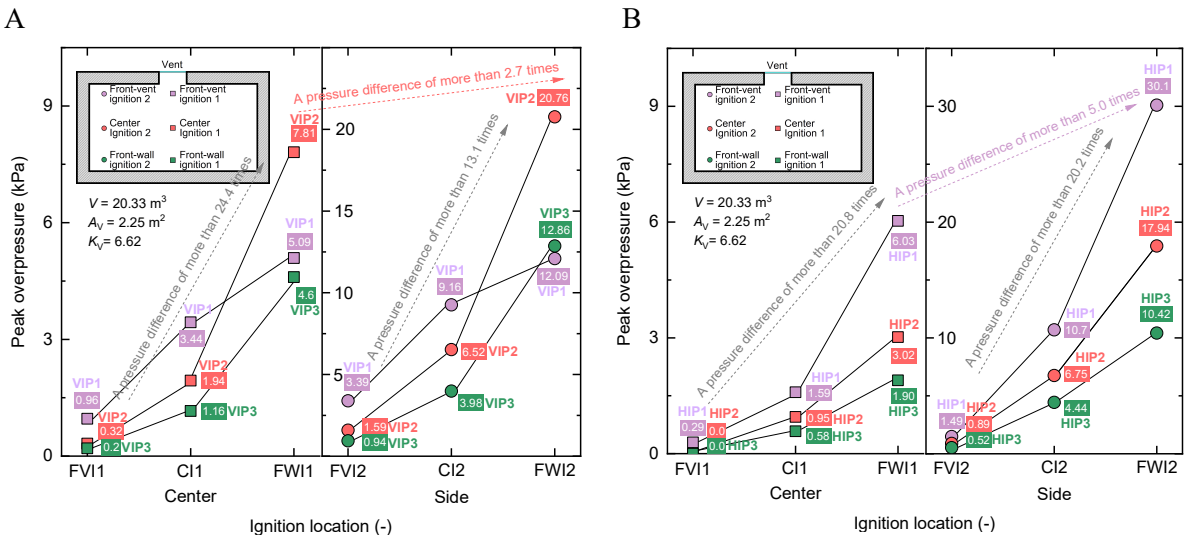

Figure 8. Peak overpressure according to ignition location
A: vertical incident pressure, B: horizontal incident pressure

3.4 Effect of Ignition Location on External Flame Behavior

We divided the results of external flame behavior according to ignition location into central (FVI1, CI1, and FWI1) and side (FVI2, CI2, and FWI2) ignition tree data, and present them in Fig. 9(a)–(f). We observed that the flame formed by the explosion of the hydrogen-air mixture inside the compartment was vented outside through the vent in the following 3 stages: (1) formation of a fireball due to the rapid combustion of the combustible cloud formed near the vent, (2) expansion of the flame to its maximum size within a few seconds, and (3) formation of a flame jet as it was pushed downward by the high-speed vented outflow.

Fig. 9(a)–(f) clearly shows the differences in the behavior of the generated external flame among each ignition location in the central (FVI, CI, and FWI) and side (FVI2, CI2, and FWI2) ignition trees. We determined that ignition at FWI and FVI resulted in the maximum and minimum fireball sizes, respectively. We also observed that the longest flame length was generated under CI and FWI ignition, whereas the opposite result was observed under FVI ignition. Comparing between the central and side ignition trees, we found that when the central ignition tree was used the length of the generated flame was longer, forming a long cylindrical column. In contrast, when the side ignition tree was used, the flame formed a lower but wide mushroom cloud shape. These results confirmed that the ignition location had a considerable impact on external flame behavior.

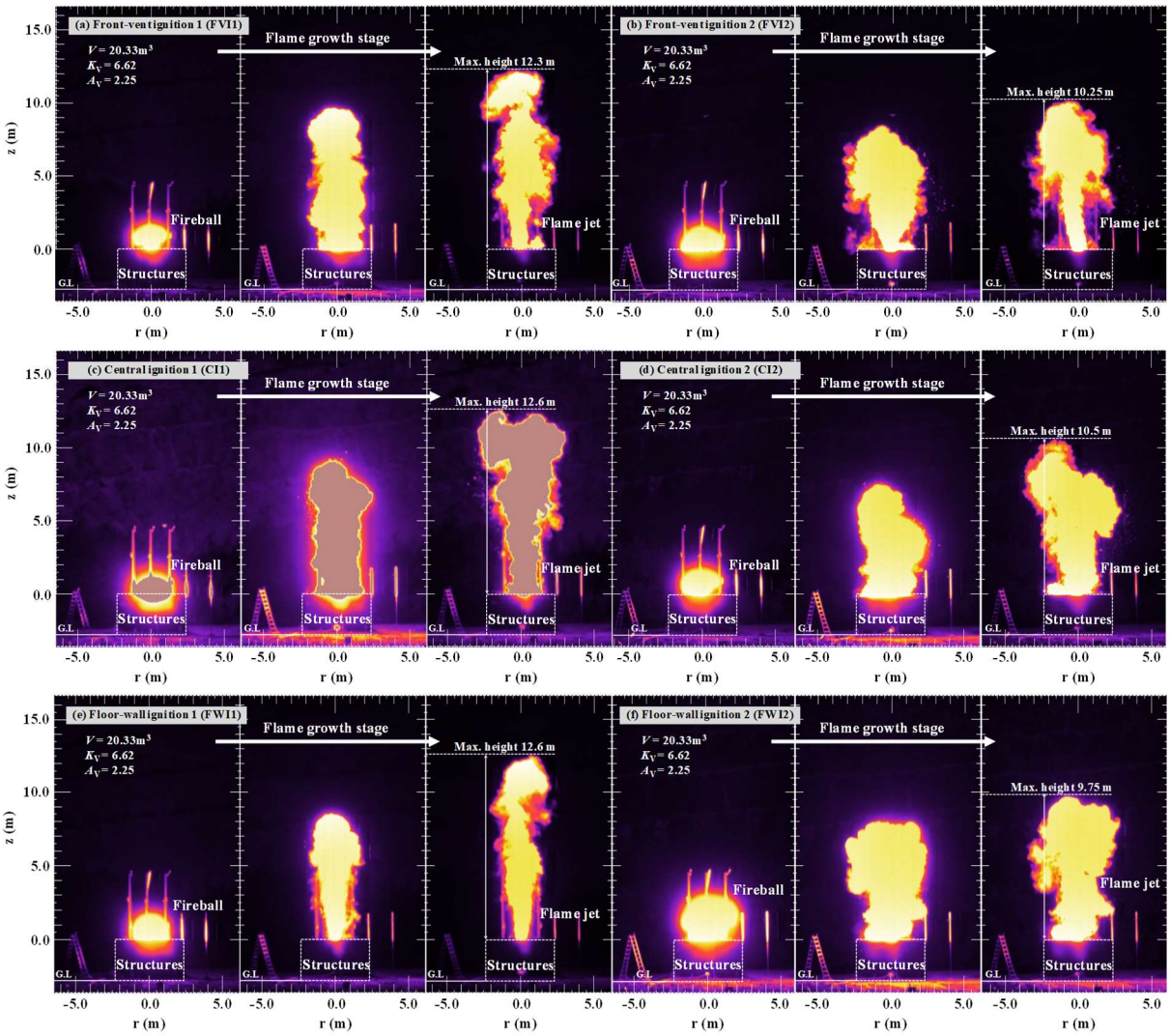

Figure 9. Effect of ignition location on external flame behavior

3.5 Damage Effect on Humans from Vent Explosions

Overpressure caused by the vent explosion of a hydrogen-air mixture inside a structure can cause damage to the human body. It is the blast wave that does most of the damage. Such damage caused by a blast wave can be represented by overpressure and impulse, with the equivalent pressure $\overline{P}$ and equivalent impulse $\overline{i}$ being given by Eq. (2) and (3). These effects can also be represented by a graph, as shown in Fig. 10 [19,20].

$$\overline{P} = \frac{P}{p_0} \tag{2}$$

$$\overline{i} = \frac{i}{p_0^{1/2} \times m^{1/3}} \tag{3}$$

where $\overline{P}$ – scaled overpressure; P – actual pressure acting on the body; P_0 – atmospheric pressure; $\overline{i}$ – scaled impulse; i – impulse; m – mass of the body.

The level of human damage based on the measured horizontal incident pressure values in this study is shown in Fig. 10 for each ignition condition. We found that under FWI2 ignition, human damage ("Injury" level) can occur at distances of HIP1 and HIP2. We predicted a 1 % fatality probability at HIP1 with a maximum overpressure of 30.01 kPa, whereas identified a 1 % probability of eardrum rupture at HIP2 with 17.94 kPa. Regarding the rest ignition conditions, we predicted minimum

damage to humans as the overpressure values measured were low. These results demonstrated that the threat of damage to humans due to overpressure would be the greatest under FWI2 ignition, further suggesting that the location of ignition source has a large impact on overpressure.

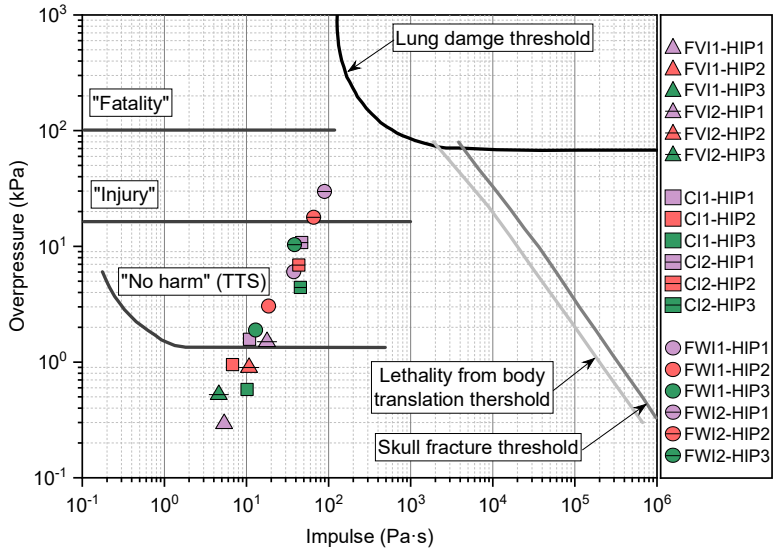

Figure 10. Overpressure-impulse thresholds of harm criteria for humans

4. CONCLUSIONS

In this study, we conducted experiments to determine the effects of vent explosions according to the location of the ignition source in a cuboid concrete structure (20.33 m^3) with a vent (1.13 m^2) on its roof, filled with a hydrogen-air mixture (29.0 vol.%). The main conclusions are summarized as follows.

We confirmed that with the increasing distance of the ignition source from the vent, the impact on overpressure and flame behavior increases, resulting in up to 24.4 times greater incident pressure values and up to 8.7 times greater reflected pressure values.

When exploring the behavior of the generated external flame, we observed that the shape of the formed flame differed according to the ignition location. In particular, the central ignition tree formed a flame with a long cylindrical column shape, whereas the side ignition tree formed a flame with a wide mushroom cloud shape.

We predicted that distant ignition (FWI2, side ignition tree) might result in "Injury" level damage to humans (1 % fatality probability) at a distance of 2.4 m away from the vent (HIP1), whereas almost no damage will occur at a distance of 7.4 m or more away from the vent.

The results of this study are used as basic data for presenting design guidelines for explosion vents in underground spaces.

ACKNOWLEDGMENTS

Research for this paper was carried out under the KICT Research Program (Project no. 20230104-001, Development of technology to secure safety and acceptability for infrastructure in hydrogen city) funded by the Ministry of Science and ICT.

REFERENCES

1. Cheon, Y., Review of Global Carbon Neutral Strategies and Technologies, *Journal of The Korean Society of Mineral and Energy Resources Engineers*, **59**, No. 1, 2022, pp. 99-112.

2. Major Projects and Future Considerations in 2020 According to the Hydrogen Economy Revitalization Road Map, 2019, National Assembly Budget Office, No.7, ISSN 2672-0280.
3. Leap to become a World-Class Hydrogen Economy Leader–Government, Hydrogen Economy Revitalization Road Map Announcement, 2019, Ministry of Trade, Industry and Energy.
4. Bauwens, C.R., Chaffee, J. and Dorofeev, S.B., Vented Explosion Overpressures from Combustion of Hydrogen and Hydrocarbon Mixtures, *Int. J. Hydrogen Energy*, **36**, No. 3, 2011, 2329-2336.
5. Bauwens, C.R., Chao, J. and Dorofeev, S.B., Effect of Hydrogen Concentration on Vented Explosion Overpressures from Lean Hydrogen-Air Deflagrations, *Int. J. Hydrogen Energy*, **36**, No. 22, 2012, 17599-17605.
6. Wang, J., Guo, J., Yang, F., Zhang, J. and Lu, S., Effect of Hydrogen Concentration on the Vented Deflagration of Hydrogen-Air Mixtures in a 1-m^3 Vessel, *Int. J. Hydrogen Energy*, **43**, No. 45, 2018, 21161-21168.
7. Skjold, T., Hisken, H., Lakshmipathy, S., et al., Vented Hydrogen Deflagrations in Containers: Effect of Congestion for Homogeneous and Inhomogeneous Mixtures, *Int. J. Hydrogen Energy*, **44**, No. 17, 2019, 8819-8832.
8. Li, P., Huang, P., Liu, Z., et al., Experimental Study on Vented Explosion Overpressure of Methane/Air Mixtures in Manhole, *Journal of Hazardous Materials*, **374**, 2019, 349-355.
9. Tang, Z., Li, J., Guo, J., et al., Effect of Vent Size on Explosion Overpressure and Flame Behavior during Vented Hydrogen-Air Mixture Deflagrations, *Nuclear Engineering and Design*, **361**, 2020, 110578.
10. Liu, W., Guo, J., Zhang, J., et al., Effect of Vent Area on Vented Deflagration of Hydrogen-Methane-Air Mixtures, *Int. J. Hydrogen Energy*, **46**, No. 9, 2021, 6992-6999.
11. Schiavetti, M., Marangon, A., Carcassi, M., Experimental Study of Vented Hydrogen Deflagration with Ignition Inside and Outside the Vented volume, *Int. J. Hydrogen Energy*, **39**, No. 35, 2014, 20455-20461.
12. Rocourt, X., Awamat, S., Sochet, I., et al., Vented Hydrogen-Air Deflagration in a Small Enclosed Volume, *Int. J. Hydrogen Energy*, **39**, No. 35, 2014, 20462-20466.
13. Liang, Z., Scaling Effects of Vented Deflagrations for Near Lean Flammability Limit Hydrogen-Air Mixtures in Large Scale Rectangular Volumes, *Int. J. Hydrogen Energy*, **42**, No. 10, 2017, 7089- 7103.
14. Zhang, Q., Wang, Y., Lian, Z., Explosion Hazards of LPG-Air Mixtures in Vented Enclosure with Obstacles, *Journal of Hazardous Materials*, **334**, 2017, 59-67.
15. Guo, J., Wang, C., Liu, X., et al., Explosion Venting of Rich Hydrogen-Air Mixtures in a Small Cylindrical Vessel with Two Symmetrical Vents, *Int. J. Hydrogen Energy*, **42**, No. 11, 2017, 7644- 7650.
16. Chen, Y., Li, Z., Ji, C., et al., Effect of Hydrogen Concentration, Non-Homogenous Mixtures and Obstacles on Vented Deflagrations of Hydrogen-Air Mixtures in a 27 m^3 Chamber, *Int. J. Hydrogen Energy*, **45**, No. 11, 2020, 7199-7209.
17. NFPA, NFPA68 Standard on Explosion Protection by Deflagration Venting Code, 2013.
18. KFS, KFS720 Standard on Venting of Deflagrations Code, 1998.
19. Crowl, D. A., and Louvar, J. F., Chemical Process Safety Fundamentals with Applications (Fourth Edition), 2019, Pearson Education Inc.
20. Center for Chemical Process Safety to the American Institute of Chemical Engineers, Guidelines for Evaluating the Characteristics of Vapor Cloud Explosions, Flash Fires, and BLEVEs, 1994, American Institute of Chemical Engineers.